Comparative study of a 3CL^{pro} inhibitor and remdesivir against both major SARS-CoV-2 clades in human airway models

Maren de Vries[1*], Adil S Mohamed[1*], Rachel A Prescott[1], Ana M Valero-Jimenez[1], Ludovic Desvignes[2,3], Rebecca O'Connor[4], Claire Steppan[4], Annaliesa S. Anderson[5], Joseph Binder[6], and Meike Dittmann[1**]

[1] Department of Microbiology, New York University Grossman School of Medicine, New York 10016, USA

[2] Department of Medicine, New York University Grossman School of Medicine, New York 10016, USA

[3] Office of Science & Research, NYU Langone Health, New York 10016, USA

[4] Pfizer Discovery Sciences, Groton, CT 06340, USA

[5] Pfizer Vaccine Research and Development, Pearl River, NY 10695, USA

[6] Pfizer Oncology Research and Development, San Diego, CA 92128, USA

* authors contributed equally

** corresponding author

Abstract

Severe acute respiratory syndrome coronavirus 2 (SARS-CoV-2) is the etiological agent of Coronavirus Disease 2019 (COVID-19), a pandemic that has claimed over 700,000 human lives. The only SARS-CoV-2 antiviral, for emergency use, is remdesivir, targeting the viral polymerase complex. PF-00835231 is a pre-clinical lead compound with an alternate target, the main SARS-CoV-2 protease $3CL^{pro}$ (M^{pro}). Here, we perform a comparative analysis of PF-00835231 and remdesivir in $A549^{+ACE2}$ cells, using isolates of two major SARS-CoV-2 clades. PF-00835231 is antiviral for both clades, and, in this assay, statistically more potent than remdesivir. A time-of-drug-addition approach delineates the timing of early SARS-CoV-2 life cycle steps and validates PF-00835231's time of action. Both PF-00835231 and remdesivir potently inhibit SARS-CoV-2 in human polarized airway epithelial cultures. Thus, our study provides *in vitro* evidence for the potential of PF-00835231 as an effective antiviral for SARS-CoV-2, addresses concerns from non-human in vitro models, and supports further studies with this compound.

Introduction

In December 2019, multiple cases of severe pneumonia with unexplained etiology were reported in Wuhan, China[1]. The infectious agent was identified as a novel member of the family *Coronaviridae*[1], later named severe acute respiratory syndrome coronavirus 2 (SARS-CoV-2)[2], and the disease it is causing was named Coronavirus Disease 2019 (COVID-19), which has since spread globally. At the time of writing, there are 751,910 deaths among 20,739,537 confirmed cases in 188 countries[3]. The only directly-acting antiviral drug, with emergency use authorization, to treat SARS-CoV-2 infections is remdesivir, a nucleoside analog that is incorporated into viral RNA by the viral polymerase, resulting in chain termination[4]. It remains a strategic priority to increase our arsenal of effective antiviral SARS-CoV-2 drugs by developing novel compounds with minimal side effects and alternate viral targets.

One such alternate SARS-CoV-2 target is its main protease, $3CL^{pro}$ (M^{pro}), which plays an essential role in the viral life cycle: Upon entry and uncoating of the viral particles, the positive stranded RNA genome is rapidly translated into two polyproteins which are subsequently processed into functional proteins by $PL2^{pro}$ and $3CL^{pro}$ viral proteases[5]. $3CL^{pro}$ is the main protease and is responsible for releasing 11 of the 13 individual proteins, including the polymerase subunits, enabling their proper folding and assembly into the active polymerase complex[6]. Thus, blocking $3CL^{pro}$ activity would effectively shut down the life cycle before viral transcription or replication can occur, making it an enticing target for intervention[7]. In addition, $3CL^{pro}$ has a unique substrate preference (Leu-Gln ↓ {Ser, Ala, Gly}), a preference not shared by any known human protease, implying the potential for high selectivity and low side effects of $3CL^{pro}$-targeting drugs[8].

Although there have been intense efforts to develop 3CL^{pro} inhibitors specific for SARS-CoV-2[7–13], no such compounds have yet been approved.

In response to a previous epidemic coronavirus in 2003, PF-00835231 was initially designed as an inhibitor of the SARS-CoV 3CL^{pro} protease[10], but, with disease declining, clinical studies were not practical and, consequently, PF-00835231 was never tested clinically. Because 3CL^{pro} of SARS-CoV and SARS-CoV-2 are 96% identical at the amino acid level, including 100% identity within the catalytic pocket[8], PF-00835231 may inhibit SARS-CoV-2 as well. Since the discovery of SARS-CoV-2, limited evolution had been observed. The two major lineages of SARS-CoV-2 circulating globally as of time of writing are represented by the Wuhan basal clade and the spike protein D614G clade, also referred to as clades A and B, respectively[14]. Compared to clade A, clade B isolates carry a mutation in ORF S, encoding the spike protein, which results in amino acid substitution D614G. D614G is frequently accompanied by an additional mutation in ORF 1b, which encodes the RNA-dependent RNA-polymerase complex (RdRp), resulting in substitution P323L in NSP12[15]. Clade B viruses are more prevalent globally, but whether this is due to a founder effect or due to functional differences remains to be determined[16]. Here, we aimed to characterize the antiviral potency and cytotoxicity profile of PF-00835231 in comparison to remdesivir, in a human type II alveolar epithelial cell line, using clinical isolates representing the two major clades, SARS-CoV-2 USA-WA1/2020 and USA/NYU-VC-003/2020 (D614G), as well as in polarized human airway epithelial cultures (SARS-CoV-2 USA-WA1/2020). Our *in vitro* studies identify PF-00835231 as a compound with better potency than other SARS-CoV-2 3CL^{pro} inhibitors described to date and similar or better potency than remdesivir.

Results

Establishing A549^{+ACE2} cells as a tool to determine SARS-CoV-2 infection and cytopathic effect by high-content microscopy. The human adenocarcinomic alveolar epithelial cell line A549 is a workhorse cell line in the study of respiratory viruses. However, A549 cells are not permissive to SARS-CoV-2 infection, as they do not highly express the SARS-CoV-2 receptor ACE2[17]. To make A549 cells amenable for experiments with SARS-CoV-2, we generated a stable A549 cell line expressing ACE2 exogenously. We confirmed elevated levels of ACE2 mRNA in A549^{+ACE2} cells by RT-qPCR, and of ACE2 protein by Western blot, flow cytometry and confocal microscopy (Fig. S1a-e). To determine permissiveness, we infected A549 or A549^{+ACE2} cells with a serial dilution of SARS-CoV-2, in a 96-well format, for 24 or 48 h. Using immunofluorescence staining for SARS-CoV-2 nucleocapsid protein (N) and high-content microscopy, we found A549^{+ACE2} cells permissive to SARS-CoV-2 infection, whereas parent A549 cells were not (Fig. S1f). Additionally, in A549^{+ACE2} cells, the percentage of infected cells increased over time, suggesting *de novo* virus production and spread (Fig. S1g). Finally, we observed that the cytopathic effect (CPE) caused by SARS-CoV-2 on A549^{+ACE2} cells manifests in syncytia formation, in which the nuclei form a ring-like structure (Fig. S1h), similar to what has been described for other coronaviruses[18,19]. Altogether, our data establish A549^{+ACE2} cells as a tool to study SARS-CoV-2 infection, spread, and cytopathic effect.

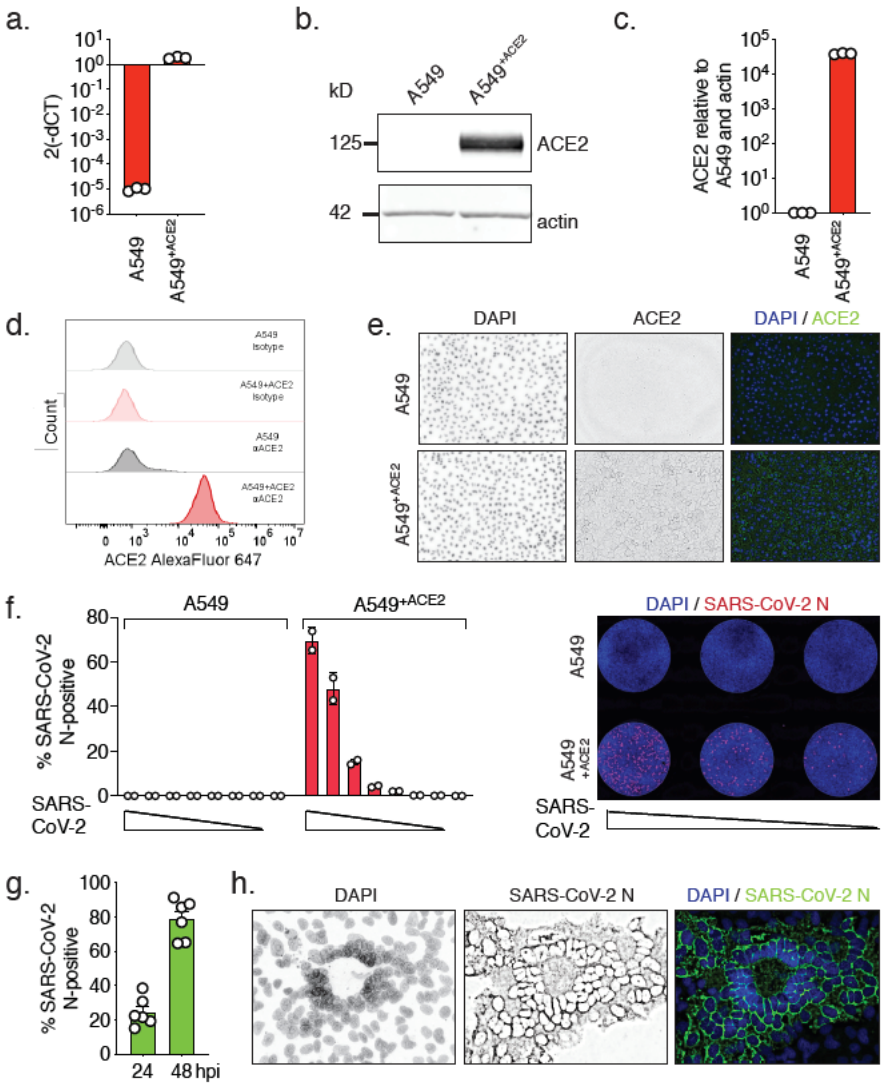

Supplemental Figure 1. Validation of A549^{+ACE2} cells as a tool to study SARS-CoV-2. A549^{+ACE2} cells were generated by lentiviral transduction delivering an ACE2 overexpression construct and subsequent bulk-selection. **a.-e.** ACE2 expression in A549 parental or A549^{+ACE2} cells determined by RT-qPCR (**a.**), western blot (**b.,** quantified in **c.**), flow cytometry (**d.**), or microscopy (**e.**). **f.** A549 parental or A549^{+ACE2} cells were infected with a serial dilution of SARS-CoV-2 USA-WA1/2020. At 24 h, cells were fixed, stained for SARS-CoV-2 N protein, and infected cells were quantified by high-content microscopy. **g.** A549 parental or A549^{+ACE2} cells were infected with SARS-CoV-2 USA-WA1/2020. At 24 and 48 h, infected cells were quantified as described in (**f.**). **h.** Confocal microscopy of SARS-CoV-2 syncytia formation in A549^{+ACE2} cells at 48 hpi.

In A549^{+ACE2} cells, PF-00835231 potently inhibits clinical SARS-CoV-2 isolates from the two major clades. PF-00835231 is a pre-clinical small molecule inhibitor of the SARS-CoV-2 protease 3CL^{pro} (M^{pro})[10]. To determine whether PF-00835231 inhibits SARS-CoV-2 in A549^{+ACE2} cells, we performed antiviral activity and cytotoxicity assays. We challenged A549^{+ACE2} cells with the clinical SARS-CoV-2 isolate USA-WA1/2020, which falls into SARS-CoV-2 clade A (GenBank accession no. MT233526). We measured virus antigen (N) expression by high-content microscopy in cells exposed to a range of drug doses at 24 or 48 hours post infection (hpi, Fig. 1a). In parallel, we determined cellular viability by measuring ATP levels in drug-treated, but uninfected cells. Remdesivir inhibited SARS-CoV-2 with an average 50% effective concentration (EC_{50}) of 0.442 µM at 24 h, and 0.238 µM at 48 h, with no significant cytotoxicity (Fig. 1b, d). In comparison, PF-00835231 was statistically more potent than remdesivir, with an EC_{50} of 0.221 µM at 24 h (p=0.0017 vs remdesivir), and 0.158 µM at 48 h (p=0.036 vs remdesivir), and showed no detectable cytotoxicity (CC_{50} > 10 µM; Fig. 1c, d).

To determine the efficacy of PF-00835231 against a SARS-CoV-2 clade B representative, we tested clinical isolate USA/NYU-VC-003/2020, which we had isolated in March 2020 (GenBank accession no. MT703677). USA/NYU-VC-003/2020 carries both of the signature clade B amino acid changes, S D614G and NSP12 P323L. PF-00835231 potently inhibited USA/NYU-VC-003/2020 in A549^{+ACE2} cells, with an EC_{50} of 0.184 µM (CC_{50} >10 µM), whereas remdesivir was inhibitory with an EC_{50} of 0.283 µM (p=0.028 vs. PF-00835231, CC_{50} >10 µM; Fig. 1 e-g). Thus, while PF-00835231 had similar antiviral activities against representative isolates of both major SARS-CoV-2

lineages in this assay, remdesivir exhibited statistically significant weaker antiviral activity against the clade A isolate compared to the clade B isolate ($p<0.05$).

Finally, we analyzed microscopy data for inhibition of the CPE that leads to ring-shaped syncytia formation. Both PF-00835231 and remdesivir decreased the overall number of infected foci, and fully protected A549^{+ACE2} cells from ring syncytia formation, at 0.33 µM and above (Fig. 1h). Collectively, we show that, in this assay, PF-00835231 inhibits isolates from both major SARS-CoV-2 lineages at similar or better effective

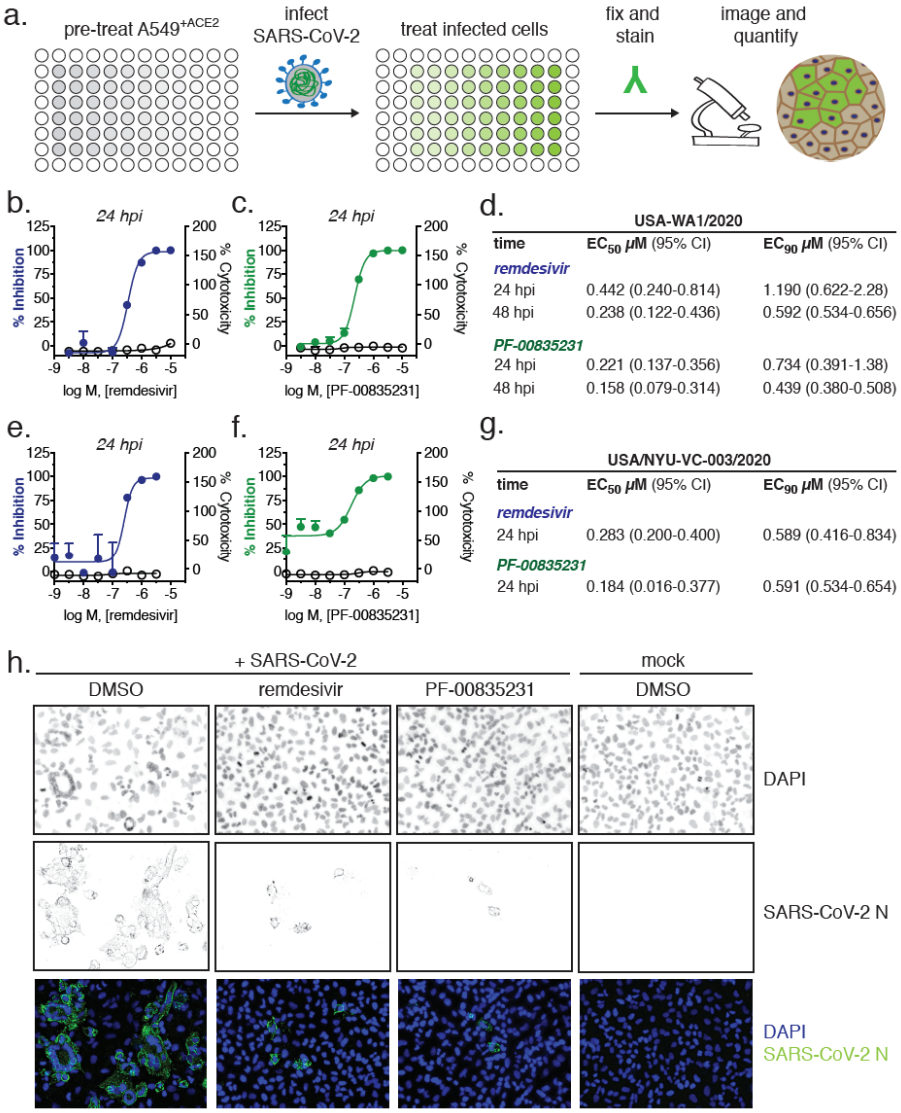

concentrations than the only currently available SARS-CoV-2 drug, remdesivir.

Figure 1. Cytotoxicity and antiviral SARS-CoV-2 activity of PF-00835231 and remdesivir in A549^{+ACE2} cells. a. Antiviral assay workflow. A549^{+ACE2} cells were infected with SARS-CoV-2 and treated with serial dilutions of PF-00835231 or remdesivir. At 24 or 48 h, cells were fixed, stained for SARS-CoV-2 N protein, and infected cells quantified by high-content microscopy. Cytotoxicity was measured in similarly treated but uninfected cultures via CellTiter-Glo assay. **b.** Remdesivir and **c.** PF-00835231 antiviral activity and cytotoxicity in A549^{+ACE2} cells infected with SARS-CoV-2 USA-WA1/2020. Representative graph of one experiment in duplicate shown. **d.** Summary of remdesivir and PF-00835231 antiviral activity against SARS-CoV-2 isolate USA-WA1/2020 from n=3 independent experiments. hpi, hours post infection; CI, confidence interval. **e.** Remdesivir and **f** PF-00835231 antiviral activity and cytotoxicity in A549^{+ACE2} cells infected with SARS-CoV-2 USA/NYU-VC-003/2020. Representative graph of one experiment in duplicate shown. **g.** Summary of remdesivir and PF-00835231 antiviral activity against SARS-CoV-2 isolate USA/NYU-VC-003/2020 from n=3 independent experiments. **h.** Representative images of SARS-CoV-2 USA-WA1/2020 syncytia formation at 48 hpi in A549^{+ACE2} cells under remdesivir or PF-00835231 treatment at the 0.33 µM dose.

Timing of PF-00835231 antiviral action against USA-WA1/2020 in A549^{+ACE2} cells is consistent with PF-00835231's role as a 3CL^{pro} inhibitor. PF-00835231 and remdesivir target different SARS-CoV-2 proteins[10,20]. PF-00835231 targets 3CL^{pro}, blocking polyprotein processing and thus formation of the viral polymerase complex[21]. Remdesivir acts on the subsequent step, which is the incorporation of nucleotides into nascent viral RNA transcripts and genomes by the viral polymerase complex[4,22]. To determine whether the action of PF-00835231 is consistent with its role as a 3CL^{pro} inhibitor, and to delineate the timing of early SARS-CoV-2 life cycle stages in A549^{+ACE2}

cells, we performed time-of-drug-addition experiments[23]. This approach determines how long the addition of a drug can be delayed before the drug loses antiviral activity. Using one-hour-increments (from 1 h prior to 4 h post infection), we varied the time-of-drug-addition for a monoclonal neutralizing antibody (a control targeting the attachment step in the viral life cycle), the drug GC-376 (a control drug for $3CL^{pro}$ inhibition, licensed for veterinary use in feline coronavirus infections[24], and recently shown to inhibit SARS-CoV-2[12]), PF-00835231, and remdesivir. We measured the percentage of SARS-CoV-2-infected cells via high-content microscopy at 12 h post-infection, which corresponds to one replication cycle in $A549^{+ACE2}$ cells, as determined previously. We synchronized infection using a preincubation step at 4°C, followed by a transition to 37°C at 1 h post-addition of virus, and used the minimum treatment doses for each drug that led to undetectable infection levels – 3 µM for PF-00835231 and the neutralizing antibody, and 10 µM for remdesivir and GC-376. The neutralizing antibody lost its antiviral function first, starting at the first addition point post-infection (1 h), confirming blockage of attachment and entry as the mode of antiviral action (Fig. 2). Interestingly, all three treatments, GC-376, PF-00835231, and remdesivir lost antiviral action at the same time of addition, starting at 2 hpi, and with more pronounced loss of activity at 3 and 4 hpi (Fig. 2). This suggests that both polyprotein processing and the start of viral transcription / translation follow each other very closely in time. These time-of-drug-addition experiments confirm the timing of PF-00835231 antiviral action as consistent with its role as a $3CL^{pro}$ inhibitor, and delineate the timing of the SARS-CoV-2 life cycle events in the tissue culture model of $A549^{+ACE2}$ cells. Furthermore, these experiments demonstrate that polymerase and protease inhibitors such as PF-00835231 can

effectively block SARS-CoV-2 replication in cells when administered within a few hours after infection has already taken place.

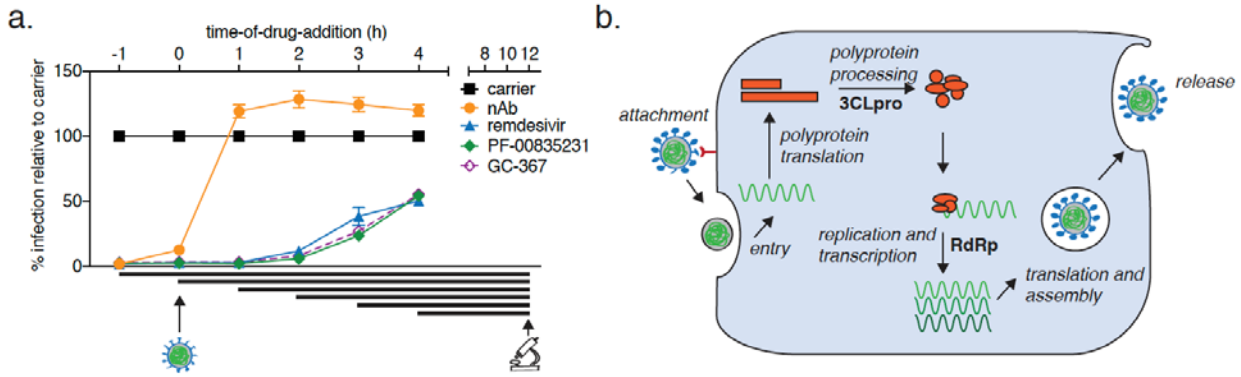

Figure 2. Time-of-drug-addition assay for PF-00835231 and remdesivir in A549^{+ACE2} cells. a. At the indicated time points, A549^{+ACE2} cells were infected with SARS-CoV-2 USA-WA1/2020, treated with 3 µM monoclonal neutralizing antibody (control targeting attachment and entry), 10 µM of the drug GC-376 (control drug for 3CL^{pro} inhibition), 3 µM PF-00835231, or 10 µM remdesivir. At 12 h (one round of replication) cells were fixed, stained for SARS-CoV-2 N protein, and infected cells quantified by high-content microscopy. Data from n=3 independent experiments. **b.** Schematic of SARS-CoV-2 life cycle steps in A549^{+ACE2} cells.

PF-00835231 is well-tolerated in polarized human airway epithelial cultures (HAEC). The human respiratory tract is a major entry portal for viruses, including SARS-CoV-2, and the first battle between host and virus occurs in cells of the respiratory epithelium. This specialized tissue contains four major cell types (basal, secretory club, goblet, and ciliated) which are organized in a characteristic polarized architecture. Human airway epithelial cultures (HAEC) recapitulate much of the complexity and architecture of this tissue (Fig. 3 a,b), and thus make it arguably one of the most physiologically relevant human tools with which we study respiratory pathogens *in vitro*.

HAEC are permissive to SARS-CoV-2 infections and were utilized to obtain the very first SARS-CoV-2 isolate in December 2019[1].

To establish the use of PF-00835231 in HAEC, we first determined its cytotoxicity profile and compared it to that of remdesivir. We added PF-00835231 or remdesivir to HAEC basolaterally (Fig. 3a), and determined tissue morphology by histology, expression of apoptosis markers by RT-qPCR, and disruption of the epithelial layer by measuring trans-epithelial resistance (TEER; Fig. S2a-d). Neither drug caused measurable adverse effects on the morphology of the cultures (Fig. S2a,b) or triggered expression of apoptosis markers (Fig. S2c). However, remdesivir, more so than PF-00835231, negatively impacted trans-epithelial resistance over time (albeit not statistically significantly), suggesting that PF-00835231 may be better-tolerated by HAEC than remdesivir (Fig. S2d).

To complement these data from differentiated HAEC with a more standardized assay, we treated a monolayer of basal-like undifferentiated precursor cells with a dose range of PF-00835231 or remdesivir for 48 hours, and quantified ATP as a measure of cell viability, similar to previous experiments with $A549^{+ACE2}$ cells. We did not detect a decrease in ATP upon PF-00835231 treatment, even at the highest amount of drug (10 µM) tested. In contrast, 10 µM of remdesivir caused a dose-dependent reduction in ATP levels, albeit not statistically significantly (Fig. S2e). These experiments demonstrate that PF-00835231 has a favorable cytotoxicity profile in our model of the polarized human airway epithelium.

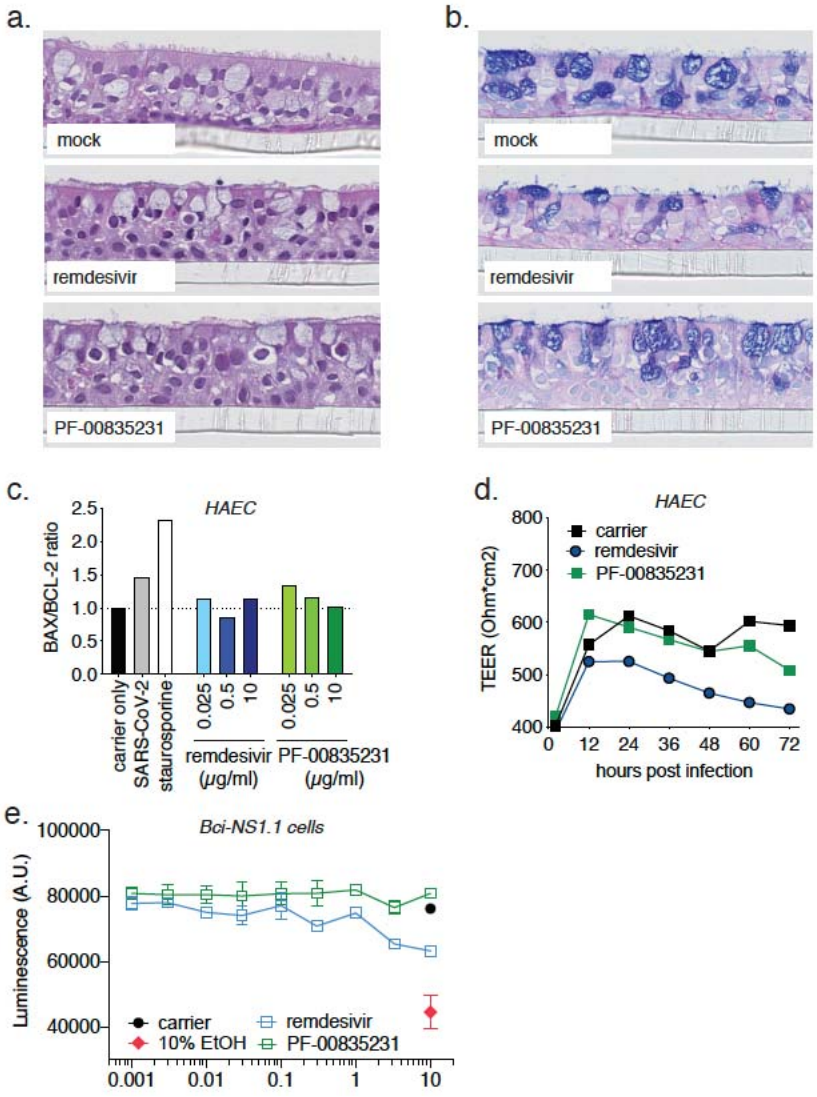

Supplemental Figure 2. Cytotoxicity of PF-00835231 and remdesivir in polarized human airway epithelial cultures (HAEC). a.,b. Representative cross-sections of uninfected HAEC, 72 h post treatment with 10 µM PF-00835231 or 10 µM remdesivir. H&E (**a.**) or PAS-Alcian blue staining (**b.**). **c.** BAX/BCL-2 ratio in drug-treated HAEC as a measure of cell death determined by RT-qPCR. DMSO as carrier control, staurosporine as positive control inducing cell death. **d.** Trans-epithelial resistance (TEER) in drug-treated, uninfected HAEC over time as a measure of epithelial integrity. Data from n=3 independent experiments. **e.** CellTiter-glo assay on undifferentiated, basal-like cell monolayers. Data from n=3 independent experiments.

In HAEC, PF-00835231 exhibits potent anti-SARS-CoV-2 USA-WA1/2020 activity. To determine PF-00835231's anti-SARS-CoV-2 activity in HAEC, we added either 0.025, 0.5 or 10 µM PF-00835231 or remdesivir, or DMSO carrier control, to the basolateral chamber of HAEC (Fig. 3a). We then challenged HAEC apically with SARS-CoV-2 USA-WA1/2020 (Fig. 3a), and determined viral infectious titers from apical washes collected at 12-hour increments. Both PF-00835231 and remdesivir potently inhibited SARS-CoV-2 titers in a dose-dependent manner, with the 10 µM dose resulting in viral titers below the limit of detection (Fig. 3c,d).

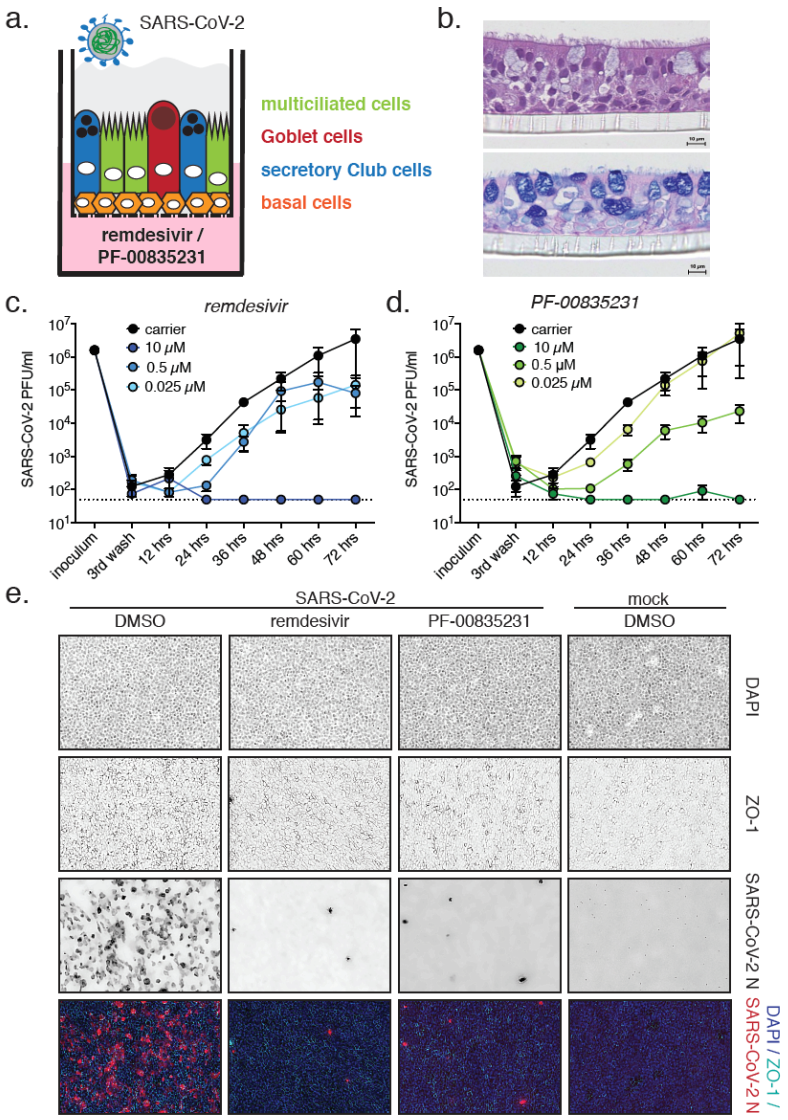

Figure 3. Comparative anti-SARS-CoV-2 activity of PF-00835231 and remdesivir in polarized human airway epithelial cultures (HAEC). a. Schematic representation of a trans-well containing a polarized HAEC in air-liquid interface. To test for antiviral activity, drugs were added to the basolateral chamber, cultures infected with SARS-CoV-2 USA-WA1/2020 from the apical side, and apical washes collected in 12 h increments to determine viral titers by plaque assay. Orange, basal cells; blue, goblet cells; green, ciliated cells; red, secretory club cells; grey, mucus. **b.** Representative cross-sections of HAEC prior to infection. H&E (upper panel) or PAS-Alcian blue staining (lower panel). **c, d.** SARS-CoV-2 USA-WA1/2020 infectious titers from HAEC treated with incremental doses of remdesivir (**c**) or PF-00835231 (**d**). **e.** Representative top views of HAEC at 72 hpi. Blue, DAPI (nuclei); cyan, ZO-1 (tight junctions); red, SARS-CoV-2 N protein (infected).

To visualize SARS-CoV-2 infection in HAEC during drug treatment, we fixed infected HAEC at the 72 h endpoint and stained them for SARS-CoV-2-N-expressing cells (Fig. 3e). In carrier control cultures, we observed robust infection. Upon treatment with 10 µM PF-00835231 or remdesivir, we found in both cases the number of infected cells significantly reduced. Taken together, both remdesivir and PF-00835231 potently inhibit SARS-CoV-2 infection in our model of the polarized human airway epithelium.

Inhibiting the multi-drug transporter MDR1 does not increase efficacy of PF-00835231 *in vitro*. Previously, a hurdle in accurately determining PF-00835231's *in vitro* efficacy was the action of the multi-drug transporter MDR1 (also known as P-Glycoprotein, encoded by *MDR1 / ABCB1*) in Vero E6 cells[10]. Vero E6 cells express high levels of the transporter. MDR1 efficiently exports PF-00835231, thereby reducing intracellular PF-00835231 levels, resulting in an under-representation of the true

antiviral activity of the compound in these cells. To determine a potential role of MDR1 transporter in our *in vitro* human airway models, we measured PF-00835231 anti-SARS-CoV-2 activity in the presence or absence of MDR1-inhibitor CP-100356. We observed no statistically significant changes in antiviral activity when blocking MDR1 activity (Fig. S3), suggesting that this transporter does not play a role in our human model systems. Our findings highlight the importance of using appropriate *in vitro* model systems in order to characterize antiviral drugs.

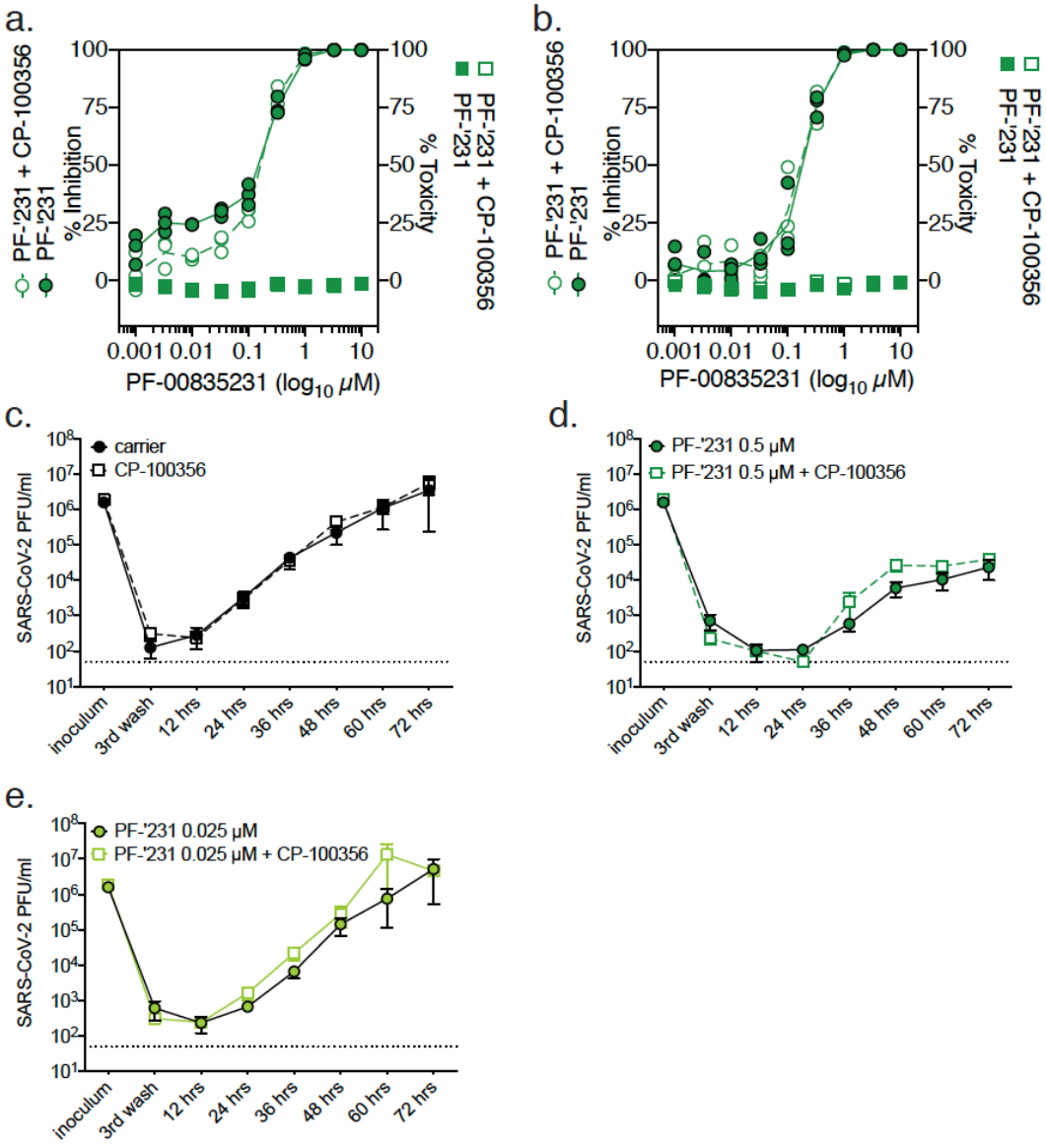

Supplemental Figure 3. Cytotoxicity and antiviral SARS-CoV-2 activity of PF-00835231 in the presence or absence of MDR1 drug exporter activity. a. PF-00835231 antiviral activity and cytotoxicity in $A549^{+ACE2}$ cells infected with SARS-CoV-2 USA-WA1/2020, in the presence or absence of 1 µM MDR1 inhibitor CP-100356. Assay performed as in Figure 1. Data from n=3 independent experiments. **b.** Apical SARS-CoV-2 USA-WA1/2020 infectious titers from HAEC treated basolaterally with 0, 0.025, or 0.5 µM PF-00835231 in the presence or absence of 1 µM MDR1 inhibitor CP-100356. Data from n=3 independent experiments.

Discussion

The current public health emergency caused by COVID-19 has illustrated our dire need for vaccines and therapeutics to combat SARS-CoV-2. In theory, each step of the SARS-CoV-2 life cycle is a potential target for antiviral intervention by small molecule inhibitors[9]. However, at the time of writing, the only antiviral drug authorized and recommended for emergency use in COVID-19 is remdesivir. Here, we report the potent antiviral activity of the protease inhibitor PF-00835231 against SARS-CoV-2 in human lung epithelial cells and a model of polarized human airway epithelial cultures (HAEC). We show that PF-00835231 has significantly better potency than remdesivir in our $A549^{+ACE2}$ cell assay, whereas in human airway epithelial cultures, we find both remdesivir and PF-00835231 similarly potent. How the potencies of either drug may relate to differences in treatment effectiveness *in vivo* is yet to be determined. We also demonstrate that PF-00835231's antiviral activity holds for viral isolates from different lineages of SARS-CoV-2.

The SARS-CoV-2 polymerase complex is the target of the majority of small molecule inhibitors in multiple stages of development for COVID-19, including remdesivir[20],

favipiravir[25], and ß-d-N4-hydroxycytidine[26]. In contrast to those compounds, PF-00835231 blocks the SARS-CoV-2 $3CL^{pro}$ protease[10]. The existence of a drug with an alternate target has important implications regarding the potential selection and management of drug resistant viral variants. First, treatment of both chronic and acute viral diseases have taught us that blocking multiple targets in combination therapy significantly decreases the likelihood for selection of viral resistance mutants[27–29]. Second, upon failure of monotherapy, it is preferable to switch to an antiviral with a different target to avoid cross-resistance[27–29]. For both scenarios, combination therapy or switching, PF-00835231 might provide an option. In coronaviruses, the genetic barrier to remdesivir or ß-d-N4-hydroxycytidine is high, as mutations conferring resistance significantly reduce viral fitness, and cross-resistance between remdesivir or ß-d-N4-hydroxycytidine has not been documented[22,26]. However, the development of a diverse toolbox of antiviral drugs with different targets to combat SARS-CoV-2 is important to further understand and control this disease.

The optimal window of opportunity for starting a successful antiviral drug regimen during acute viral infections, such as influenza, is the first few days post symptom onset, while viral replication is actively ongoing[30]. For most COVID-19 patients, this window is likely limited to the first week of symptoms[31]. Such early treatment with remdesivir is impeded by its need for intravenous (IV) administration, requiring a healthcare facility setting, though it still demonstrated benefit for 68% of patients with more advanced infection in randomized clinical studies[32]. PF-00835231 is also a potential IV treatment. However, the time of active SARS-CoV-2 replication might be prolonged in the most severe patients, as suggested by the aforementioned clinical data[32]. Thus, the usefulness of a

SARS-CoV-2 antiviral regimen even at later times of infection further supports the investigation of therapeutic efficacy of coronavirus specific $3CL^{pro}$ protease inhibitors for the treatment of COVID-19.

Early in the pandemic, protease inhibitors approved for other viruses were tested off-label in COVID-19 treatment, albeit with limited success[33]. This failure highlighted the need for novel compounds specific to the protease of coronaviruses. A number of compounds have since been identified and characterized in *in vitro* assays, including the cancer drug carmofur (1-hexylcarbamoyl-5-fluorouracil)[13], an alpha-ketoamide inhibitor named 13b[8], and others, including GC-376[34]. In cell-based assays, these compounds act at an EC_{50} in the micromolar range, whereas PF-00835231 inhibits SARS-CoV-2 with EC_{50} in the nanomolar range. In fact, our direct comparison of GC-376 and PF-00835231 in $A549^{+ACE2}$ cells (Fig. 2) showed that 10 µM of GC-367 are required to suppress SARS-CoV-2 infection completely, whereas the same is achieved with only 3 µM of PF-00835231. These results illustrate the potency of PF-00835231 compared to other $3CL^{pro}$ inhibitors.

Spillovers of zoonotic coronaviruses with high pathogenic potential into the human population are not isolated events, as repeatedly illustrated by the emergence of SARS-CoV in 2002, Middle East Respiratory Syndrome Coronavirus (MERS-CoV) in 2012, and now SARS-CoV-2 in 2019[35]. To prepare for future pandemics, the development of pan-coronavirus compounds is of strategic importance. This involves choosing viral targets that are highly conserved within the coronavirus family, such as the $3CL^{pro}$ protease[8]. Indeed, *in vitro* inhibition assays with PF-00835231 and purified $3CL^{pro}$ of SARS-CoV, SARS-CoV-2 or CoV 229E showed that PF-00835231 inhibits all three at

low nanomolar levels[10]. Work to advance this compound to needed pre-clinical *in vivo* efficacy studies is currently underway. Together, our promising results in two physiologically relevant human *in vitro* models for SARS-CoV-2 show efficient antiviral activity, address concerns arising from non-human models like Vero E6 cells, and therefore warrant additional investigations of PF-00835231 as a potential treatment for COVID-19.

Methods

Study design. The primary goal of this study was to compare the *in vitro* efficacy and cytotoxicity of PF-00835231 and remdesivir in two human model systems for SARS-CoV-2 infection, A549^{+ACE2} cells and polarized human airway epithelial cultures. Compound characterization at NYU was done in a blinded manner. If not stated otherwise, all assays were performed in n=3 biological replicates. First, we performed in-depth characterization of A549^{+ACE2} cells for the study of SARS-CoV-2, using RT-qPCR, western blotting, flow cytometry, microscopy, and high-content imaging. Second, we evaluated the *in vitro* efficacy and cytotoxicity of PF-00835231 and remdesivir in A549^{+ACE2} cells. We performed antiviral assays with SARS-CoV-2 from the two major clades at two different time points. Third, we performed time-of-drug-addition assays in A549^{+ACE2} cells to delineate the time of antiviral action for PF-00835231 and remdesivir within the SARS-CoV-2 life cycle. Fourth, we assessed the *in vitro* efficacy and cytotoxicity of PF-00835231 and remdesivir in the physiologically relevant model of polarized human airway epithelial cultures. Finally, we determined the role of efflux transporter MDR1 on the antiviral efficacy of PF-00835231. Our studies were intended

to generate the data required to justify further pre-clinical investigations as a potential treatment for COVID-19.

Cells and viruses. A549 cells were purchased from ATCC (cat no. CCL-185). To generate $A549^{+ACE2}$ cells, we cloned the human ACE2 cDNA sequence (NP_001358344.1) into a pLV-EF1a-IRES-Puro backbone vector (Addgene, cat no. 85132), and prepared lentiviral particles as described previously[36]. A549 cells were transduced with pLV-EF1α-hACE2-IRES-Puro lentivirus and bulk-selected for transduced cells using 2.5 µg/ml puromycin. $A549^{+ACE2}$ cells were maintained in DMEM (Gibco, cat no. 11965-092) containing 10% FBS (Atlanta Biologicals, cat no. S11150) (complete media), and puromycin (2.5 µg/ml final) was added to the media at every other passage. $A549^{+ACE2}$ cells were used for SARS-CoV-2 infection studies. Vero E6 cells, purchased from ATCC (cat no. CLR-1586), were maintained in DMEM (Gibco, cat no. 11965-092) containing 10% FBS (Atlanta Biologicals, cat no. S11150). Vero E6 cells were used for growing SARS-CoV-2 stocks and for SARS-CoV-2 plaque assays. Basal-like human airway progenitor cells (Bci-NS1.1[37]) were obtained from Dr. Ronald G. Crystal and maintained in BEGM Medium (Lonza, cat no. CC-3171 and CC-4175) for cytotoxicity assays, while Pneumacult Ex Plus medium (StemCell, cat no. 05040) was used to culture cells for generation of human airway epithelial cultures. Bci-NS1.1 were used for cytotoxicity assays and for generation of polarized human airway epithelial cultures (HAEC).

All SARS-CoV-2 stock preparations and following infection assay were performed in the CDC/USDA-approved BSL-3 facility in compliance with NYU Grossman School of

Medicine guidelines for biosafety level 3. SARS-CoV-2 isolate USA-WA1/2020, deposited by the Center for Disease Control and Prevention, was obtained through BEI Resources, NIAID, NIH (cat no. NR-52281, GenBank accession no. MT233526). The USA-WA1/2020 stock, obtained at passage 4, was passaged once in Vero E6 cells to generate a passage 5 working stock (1.7E + 06 PFU/mL) for our studies on A549^{+ACE2}. For studies on human airway epithelial cultures, passage 5 USA-WA1/2020 was amplified once more in Vero E6 cells and concentrated using an Amicon Ultra-15 centrifugal filter unit with a cut off of 100 kDa, resulting in a passage 6 working stock with 1.08E + 07 PFU/ml. SARS-CoV-2 USA/NYU-VC-003/2020 was isolated from a patient in March 2020, and deposited at BEI Resources, NIAID, NIH (not yet available, GenBank accession no. MT703677). The USA/NYU-VC-003/2020 passage 0 stock was passaged twice in Vero E6 to generate a passage 2 working stock (1.1E + 07 PFU/mL) for our studies on A549^{+ACE2}.

Characterization of A549^{+ACE2} cells. Confluent 6-well A549 and A549^{+ACE2} cells were washed with PBS and cells were detached with CellStripper dissociation reagent (Corning cat no. 25056CI). Cells were pelleted, washed with PBS and either i) lysed in LDS sample buffer (ThermoFisher cat no. NP0007) supplemented with reducing agent (ThermoFisher cat no. NP0004) and Western blots were performed to analyze levels of ACE2 (1:1,000, GeneTex cat no. GTX101395) with beta-actin (1:10,000, ThermoFisher cat no. MA5-15739) as the loading control and imaged using Li-Cor Odyssey CLx, or ii) incubated in FACS buffer (PBS, 5% FBS, 0.1% sodium azide, 1mM EDTA) for 30 min on ice followed by 1 hour incubation with AlexaFluor 647 conjugated anti-ACE2 (1:40,

R&D Biosystems cat no.FABAF9332R) or isotype control (1:40, R&D Biosystems cat no. IC003R) and subsequent analysis on CytoFLEX flow cytometer. Surface ACE2 was visualized by staining A549 and A549^{+ACE2} cells at 4°C with anti-ACE2 (1:500, R&D Biosystems AF933) and AlexaFluor 647 secondary antibody and DAPI. Images were collected on the Keyence BX-Z microscope. Confluent 6-well A549 and A549^{+ACE2} cells were collected in RLT lysis buffer supplemented with beta-mercaptoethanol and total RNA was extracted using Qiagen RNeasy mini kit. cDNA synthesis was performed using SuperScript™ III system (ThermoFisher cat no. 18080051) followed by RT-qPCR with PowerUp SYBR Master Mix (ThermoFisher cat no. A25742) on a QuantStudio 3 Real Time PCR System using gene-specific primers pairs for ACE2 and RPS11 as the reference gene. (ACE2fwd:GGGATCAGAGATCGGAAGAAGAAA, ACE2rev:AGGAGGTCTGAACATCATCAGTG, RPS11fwd:GCCGAGACTATCTGCACTAC, RPS11rev:ATGTCCAGCCTCAGAACTTC). A549 and A549^{+ACE2} cells were seeded in black wall 96-well plates and at confluency, cells were infected with SARS-CoV-2. At 24 and 48hpi, samples were fixed, stained with SARS-CoV-2 N mouse monoclonal SARS-CoV anti-N antibody 1C7, which cross reacts with SARS-CoV-2 N (1:1000, kind gift of Thomas Moran), AlexaFluor 647 secondary antibody and DAPI and imaged using CellInsight CX7 LZR high-content screening platform. Images were analyzed and quantified with HCS Navigator software. Syncytia were imaged using the Keyence BX-Z microscope at 60X magnification on A549^{+ACE2} cultured on chambered slides followed by 48 hpi SARS-CoV-2 infection and staining with SARS-CoV-2 N, AlexaFluor 647 secondary antibody and DAPI.

Human airway epithelial cultures (HAEC). To generate HAEC, Bci-NS1.1 were plated (7.5 E + 04 cells/well) on rat-tail collagen type 1-coated permeable transwell membrane supports (6.5 mm; Corning, cat no. 3470), and immersed apically and basolaterally in Pneumacult Ex Plus medium (StemCell, cat no. 05040). Upon reaching confluency, medium was removed from the apical side ("airlift"), and medium in the basolateral chamber changed to Pneumacult ALI maintenance medium (StemCell, cat no. 05001). Medium in the basolateral chamber was exchanged with fresh Pneumacult ALI maintenance medium every 2-3 days for 12-15 days to form differentiated, polarized cultures that resemble *in vivo* pseudostratified mucociliary epithelium. Cultures were used within 4-6 weeks of differentiation. HAEC were used for cytotoxicity assays and SARS-CoV-2 infections.

Compound acquisition, dilution, and preparation. PF-00835231, remdesivir and CP-100356 were solubilized in 100% DMSO and provided by Pfizer, Inc. Compound stocks diluted in DMSO to 30 mM were stored at -20°C. Compounds were diluted to 10 µM working concentration in complete media or Pneumacult ALI maintenance medium. All subsequent compound dilutions were performed in according media containing DMSO equivalent to 10 µM compound. As controls for the time-of-drug-addition assay, GC-376 was purchased from BPS Biosciences (cat no. 78013) and used at 10 µM working concentration, and SARS-CoV-2 (2019-nCov) rabbit polyclonal spike neutralizing antibody from Sino Biological (cat no. 40592-R001) was used at 3 µM working

471 concentration. As a positive control for cytotoxicity assays, staurosporine was
472 purchased from Sigma (cat no. S6942), and used at 1 µM working concentration.

473

474 **In vitro efficacy and cytotoxicity in A549^{+ACE2} cells.** A549^{+ACE2} cells were seeded into
475 black wall 96-well plates at 70% confluency. The next day, media was removed and
476 replaced with complete media containing compound/carrier two hours prior to infection.
477 Cells were then infected at multiplicity of infection (MOI) 0.425, based on Vero E6 titer,
478 at 37°C. 1 hour post virus addition, virus was removed, and media containing
479 compound/carrier was added. At 24 and 48 hours post infection, cells were fixed by
480 submerging in 10% formalin solution for 30-45 min. After fixation cells were washed
481 once with H_2O to remove excess formalin. Plates were dried and PBS was added per
482 well before exiting the BSL-3 facility. Fixed cells were permeabilized and stained with
483 mouse monoclonal SARS-CoV anti-N antibody 1C7, which cross-reacts with SARS-
484 CoV-2 N (kind gift of Thomas Moran), goat anti-mouse AlexaFluor 647, and DAPI.
485 Plates were scanned on the CellInsight CX7 LZR high-content screening platform. A
486 total of 9 images were collected at 4x magnification to span the entire well. Images were
487 analyzed using HCS Navigator to obtain total number of cells/well (DAPI stained cells)
488 and percentage of SARS-CoV-2 infected cells (AlexaFluor 647 positive cells). To enable
489 accurate quantification, exposure times for each channel were adjusted to 25% of
490 saturation and cells at the edge of each image were excluded in the analysis. SARS-
491 CoV-2-infected cells were gated to include cells with an average fluorescence intensity
492 greater than 3 standard deviations that of mock infected and carrier treated cells.

For determination of cytotoxicity, A549^{+ACE2} cells were seeded into opaque white wall 96-well plates. The following day, media was removed, replaced with media containing compound/carrier or staurosporine, and incubated for 24 or 48 hours, respectively. At these timepoints, ATP levels were determined by CellTiter-Glo 2.0 (Promega, cat no. G9242) using a BioTek Synergy HTX multi-mode reader.

Time-of-drug-addition experiments. A549^{+ACE2} cells seeded into black wall 96-well plates and at confluency were treated and infected as followed. At 2.5 hours prior infection cells were pre-treated with complete media containing 1x compound/carrier. In addition, SARS-CoV-2 (2x) was incubated with SARS-CoV-2 (2019-nCov) rabbit polyclonal spike neutralizing antibody (nAB, 2x). Pre-treated cells and virus/neutralizing antibody mix (1x) were incubated for 1 hour at 37°C. To synchronize infection, pre-incubated plates and SARS-CoV-2/nAB mix were chilled at 4°C for 30 min and SARS-CoV-2 was diluted on ice in media containing compound/carrier/nAB. Following pre-chilling, virus/compound/carrier/nAB mixtures were added to the cells to allow binding of virus for 1 hour at 4°C. Plates were moved to 37°C to induce virus entry and therefore infection. 1 hour post virus addition, virus was removed, and complete media was added to all wells. Complete media containing 2x compound/carrier/nAB was added to pre-treated cells, cells treated at infection and cells treated at 1 hour post infection. At 2, 3 and 4 hours post infection complete media containing compound/carrier/nAb was added to according wells. At 12 hours post infection, samples were fixed, stained with SARS-CoV-2 N, AlexaFluor 647 secondary antibody and DAPI and imaged using

515 CellInsight CX7 LZR high-content screening platform. Images were analyzed and
516 quantified with HCS Navigator software as described for in vitro efficacy in A549+ACE2.

517

518 **In vitro efficacy and cytotoxicity in human airway epithelial cultures (HAEC).** 48
519 hours prior to infection, 2-6 week old HAEC were washed apically twice for 30 min each
520 with pre-warmed PBS containing calcium and magnesium, to remove mucus on the
521 apical surface. 2 hours prior to infection HAEC were pretreated by exchanging the ALI
522 maintenance medium in the basal chamber with fresh medium containing compounds or
523 carrier. Remdesivir and PF-00835231 were used at 10, 0.5 and 0.025 µM, and CP-
524 100356 at 1 µM. 1 hour prior to infection, cultures were washed apically twice for 30 min
525 each with pre-warmed PBS containing calcium and magnesium. Each culture was
526 infected with 1.35E + 05 PFU (Vero E6) per culture for two hours at 37°C. A sample of
527 the inoculum was kept and stored at -80°C for back-titration by plaque assay on Vero
528 E6 cells. For assessment of compound toxicity, additional cultures were washed and
529 pre-treated as the infected cultures. Instead of being infected, these cultures were
530 incubated with PBS containing calcium and magnesium only as Mock treatment. HAEC
531 were incubated with the viral dilution or Mock treatment for 2 hours at 37°C. The
532 inoculum was removed and the cultures were washed three times with pre-warmed PBS
533 containing calcium and magnesium. For each washing step, buffer was added to the
534 apical surface and cultures were incubated at 37°C for 30 min before the buffer was
535 removed. The third wash was collected and stored at -80°C for titration by plaque assay
536 on Vero E6 cells. Infected cultures were incubated for a total of 72 hours at 37°C.
537 Infectious progeny virus was collected every 12 hours by adding 60 µl of pre-warmed

PBS containing calcium and magnesium, incubation at 37°C for 30 min and collection of the apical wash to store at -80°C until titration. Additionally, trans-epithelial electrical resistance (TEER) was measured in uninfected but treated HAEC to quantify the tissue integrity in response to treatment with compounds or carrier. At the end point, cultures were fixed by submerging in 10% formalin solution for 24 hours and washed three times with PBS containing calcium and magnesium before further processing for histology. Alternatively, at the end point, transwell membranes were excised and submerged in RLT buffer to extract RNA using the RNAeasy kit (Qiagen, cat no. 74104). cDNA synthesis was performed using SuperScript™ III system (ThermoFisher cat no. 18080051) followed by RT-qPCR with TaqMan universal PCR master mix (ThermoFisher cat no. 4305719) and TaqMan gene expression assay probes (ThermoFisher GAPDH cat no. 4333764F, BAX cat no. Hs00180269_m1, BCL2 cat no. Hs00608023_m1) using a QuantStudio 3 Real Time PCR System.

For additional determination of cytotoxicity in undifferentiated HAEC precursor cells, Bci-NS1.1 cells were seeded into opaque white wall 96-well plates. The following day, media was removed, replaced with media containing compound/carrier or staurosporine, and incubated for 24 or 48 hours, respectively. At these timepoints, ATP levels were determined by CellTiter-Glo 2.0 (Promega, cat no. G9242) using a BioTek Synergy HTX multi-mode reader.

Histology on human airway epithelial cultures. For histology, transwell inserts were prepared using a Leica Peloris II automated tissue processor, paraffin embedded, and sectioned at 3 µm. The resulting slides were stained using a modified Periodic acid–

Schiff (PAS)-Alcian Blue protocol (Histotechnology,Freida L. Carson). Sections were imaged on the Leica SCN whole slide scanner and files uploaded to the Slidepath Digital Image Hub database for viewing.

Immunofluorescence on human airway epithelial cultures. For Immunofluorescence of HAEC at top view, fixed and washed cultures were permeabilized with 50 mM NH_4Cl (in PBS), 0.1% w/v saponin and 2% BSA (permeabilization/blocking (PB) buffer). Cultures were stained with i) rabbit polyclonal anti-SARS Nucleocapsid Protein antibody, which cross reacts with SARS-CoV-2 N (1:1000, Rockland cat no. 200-401-A50) and goat-anti-rabbit AlexaFluor 488, to visualize infection ii) mouse monoclonal anti-ZO-1-1A12 (1:500, Thermo Fisher cat no. 33-9100) and goat anti-mouse AlexaFluor 647 to visualize tight junctions, and DAPI. All dilutions were prepared in PB buffer. Images were collected on the Keyence BX-Z microscope.

Statistical analysis. Antiviral activities of PF-00835231 and remdesivir in $A549^{+ACE2}$ cells were determined by the following method. The percent inhibition at each concentration was calculated by ActivityBase (IDBS) based on the values for the no virus control wells and virus containing control wells on each assay plate. The concentration required for a 50% / 90% response (EC_{50} / EC_{90}) was determined from these data using a 4 parameter logistic model. Curves were fit to a Hill slope of 3 when >3 and the top dose achieved ≥50% effect. Geometric means and 95% confidence intervals were generated in ActivityBase. Statistical comparisons were performed by log transforming the EC_{50} and EC_{90} values and fitting separate linear models to each

endpoint, assuming equal log-scale variances across conditions and interactions of compound with strain and compound with time. The model can be described mathematically as

$$\log \mathrm{EC}_x = Treatment_i + \varepsilon_{i,j},\ x = 50 \text{ or } 90$$

where $Treatment_i$ represents the effect of the combination of compound, strain, and time and $\varepsilon_{i,j}$ represents a normal error term for treatment i and assay replicate j. Contrasts between the factor combinations of interest were computed to assess significance and back-transformed into ratios of geometric means. Statistical significance was defined by a p value <0.05. Other statistical data analyses were performed in GraphPad Prism 7. Statistical significance for each endpoint was determined with specific statistical tests as indicated in each legend. For each test, a P-value < 0.05 was considered statistically significant.

References

1. Zhu, N. *et al.* A novel coronavirus from patients with pneumonia in China, 2019. *N. Engl. J. Med.* **382**, 727–733 (2020).
2. Gorbalenya, A. E. *et al.* The species Severe acute respiratory syndrome-related coronavirus: classifying 2019-nCoV and naming it SARS-CoV-2. *Nat. Microbiol.* **5**, 536–544 (2020).
3. Dong, E., Du, H. & Gardner, L. An interactive web-based dashboard to track COVID-19 in real time. *The Lancet Infectious Diseases* (2020). doi:10.1016/S1473-3099(20)30120-1
4. Pruijssers, A. J. *et al.* Remdesivir Inhibits SARS-CoV-2 in Human Lung Cells and Chimeric SARS-CoV Expressing the SARS-CoV-2 RNA Polymerase in Mice. *Cell Rep.* **32**, 107940 (2020).
5. Ziebuhr, J. & Siddell, S. G. Processing of the Human Coronavirus 229E Replicase Polyproteins by the Virus-Encoded 3C-Like Proteinase: Identification of Proteolytic Products and Cleavage Sites Common to pp1a and pp1ab. *J. Virol.* **73**, 177–185 (1999).
6. Gadlage, M. J. & Denison, M. R. Exchange of the Coronavirus Replicase

Polyprotein Cleavage Sites Alters Protease Specificity and Processing. *J. Virol.* **84**, 6894–6898 (2010).

7. Dai, W. *et al.* Structure-based design of antiviral drug candidates targeting the SARS-CoV-2 main protease. *Science (80-.).* **1335**, eabb4489 (2020).
8. Zhang, L. *et al.* Crystal structure of SARS-CoV-2 main protease provides a basis for design of improved a-ketoamide inhibitors. *Science (80-.).* **368**, 409–412 (2020).
9. David E. Gordon1, Gwendolyn M. Jang, Mehdi Bouhaddou, Jiewei Xu1, K. O. *et al.* A SARS-CoV-2-Human Protein-Protein Interaction Map Reveals Drug Targets and Potential Drug- Repurposing. *biorxiv* (2020).
10. Hoffman, R. L. *et al.* The Discovery of Ketone-Based Covalent Inhibitors of Coronavirus 3CL Proteases for the Potential Therapeutic Treatment of COVID-19. 1–106 (2020). doi:doi.org/10.26434/chemrxiv.12631496.v1
11. Yoshino, R., Yasuo, N. & Sekijima, M. Identification of key interactions between SARS-CoV-2 Main Protease and inhibitor drug candidates. *ChemRxiv doi:10.26434/chemrxiv.12009636.v1* 1–12 (2020). doi:10.26434/chemrxiv.12009636.v1
12. Ma, C. *et al.* Boceprevir, GC-376, and calpain inhibitors II, XII inhibit SARS-CoV-2 viral replication by targeting the viral main protease. *Cell Res.* (2020). doi:10.1038/s41422-020-0356-z
13. Jin, Z. *et al.* Structural basis for the inhibition of SARS-CoV-2 main protease by antineoplastic drug carmofur. *Nat. Struct. Mol. Biol.* **27**, 529–532 (2020).
14. Rambaut, A. *et al.* A dynamic nomenclature proposal for SARS-CoV-2 lineages to assist genomic epidemiology. *Nat. Microbiol.* (2020). doi:10.1038/s41564-020-0770-5
15. Gonzalez-Reiche, A. S. *et al.* Introductions and early spread of SARS-CoV-2 in the New York City area. *Science (80-.).* **21**, eabc1917 (2020).
16. Grubaugh, N. D., Hanage, W. P. & Rasmussen, A. L. Making Sense of Mutation: What D614G Means for the COVID-19 Pandemic Remains Unclear. *Cell* (2020). doi:10.1016/j.cell.2020.06.040
17. Daniel Blanco-Melo, Benjamin E. Nilsson-Payant, Wen-Chun Liu, Skyler Uhl, D., Hoagland, Rasmus Møller, Tristan X. Jordan, Kohei Oishi, Maryline Panis, D., Sachs, Taia T. Wang, Robert E. Schwartz, Jean K. Lim, Randy A. Albrecht1, B. & TenOever, R. Imbalanced host response to SARS-CoV-2 drives development of COVID-19. *Cell* (2020). doi:10.1016/j.cell.2020.04.026
18. Lavi, E., Wang, Q., Weiss, S. R. & Gonatas, N. K. Syncytia formation induced by coronavirus infection is associated with fragmentation and rearrangement of the Golgi apparatus. *Virology* **221**, 325–334 (1996).
19. Corver, J., Broer, R., Van Kasteren, P. & Spaan, W. Mutagenesis of the transmembrane domain of the SARS coronavirus spike glycoprotein: Refinement of the requirements for SARS coronavirus cell entry. *Virol. J.* **6**, 1–13 (2009).
20. Gordon, C. J. *et al.* Remdesivir is a direct-acting antiviral that inhibits RNA-dependent RNA polymerase from severe acute respiratory syndrome coronavirus 2 with high potency. *J. Biol. Chem.* **295**, 6785–6797 (2020).
21. Krichel, B., Falke, S., Hilgenfeld, R. & Redecke, L. Processing of the SARS-CoV pp1a / ab nsp7 – 10 region. **0**, 1009–1019 (2020).

22. Agostini, M. L. *et al.* Coronavirus Susceptibility to the Antiviral Remdesivir (GS-5734) Is Mediated by the Viral Polymerase and the Proofreading Exoribonuclease. *MBio* **9**, (2018).
23. Daelemans, D., Pauwels, R., De Clercq, E. & Pannecouque, C. A time-of-drug addition approach to target identification of antiviral compounds. *Nat. Protoc.* **6**, 925–933 (2011).
24. Kim, Y. *et al.* Broad-Spectrum Antivirals against 3C or 3C-Like Proteases of Picornaviruses, Noroviruses, and Coronaviruses. *J. Virol.* **86**, 11754–11762 (2012).
25. Shannon, A. *et al.* Favipiravir strikes the SARS-CoV-2 at its Achilles heel, the RNA polymerase. *bioRxiv* (2020). doi:10.1101/2020.05.15.098731
26. Sheahan, T. P. *et al.* An orally bioavailable broad-spectrum antiviral inhibits SARS-CoV-2 in human airway epithelial cell cultures and multiple coronaviruses in mice. *Sci. Transl. Med.* **12**, (2020).
27. Günthard, H. F. *et al.* Human Immunodeficiency Virus Drug Resistance: 2018 Recommendations of the International Antiviral Society-USA Panel. *Clin. Infect. Dis.* (2019). doi:10.1093/cid/ciy463
28. Su, T. H. & Liu, C. J. Combination therapy for chronic hepatitis B: Current updates and perspectives. *Gut and Liver* (2017). doi:10.5009/gnl16215
29. Whitley, R. J. & Monto, A. S. Resistance of Influenza Virus to Antiviral Medications. *Clin. Infect. Dis.* (2019). doi:10.1093/cid/ciz911
30. Kumar, A. Early versus late oseltamivir treatment in severely ill patients with 2009 pandemic influenza A (H1N1): Speed is life. *J. Antimicrob. Chemother.* (2011). doi:10.1093/jac/dkr090
31. Wölfel, R. *et al.* Virological assessment of hospitalized patients with COVID-2019. *Nature* (2020). doi:10.1038/s41586-020-2196-x
32. Jonathan Grein, M. D. *et al.* Compassionate Use of Remdesivir for Patients with Severe Covid-19. *N. Engl. J. Med.* (2020).
33. Cao, B. *et al.* A trial of lopinavir-ritonavir in adults hospitalized with severe covid-19. *N. Engl. J. Med.* (2020). doi:10.1056/NEJMoa2001282
34. Ma, C. *et al.* Boceprevir, GC-376, and calpain inhibitors II, XII inhibit SARS-CoV-2 viral replication by targeting the viral main protease. *Cell Res.* (2020). doi:10.1038/s41422-020-0356-z
35. Gralinski, L. E. & Menachery, V. D. Return of the coronavirus: 2019-nCoV. *Viruses* **12**, 1–8 (2020).
36. Seifert, L. L. *et al.* The ETS transcription factor ELF1 regulates a broadly antiviral program distinct from the type i interferon response. *PLoS Pathog.* (2019). doi:10.1371/journal.ppat.1007634
37. Walters, M. S. *et al.* Generation of a human airway epithelium derived basal cell line with multipotent differentiation capacity. *Respir Res* **14**, 135 (2013).

Acknowledgements

We would like to thank Thomas M Moran, Icahn School of Medicine at Mount Sinai, and Luis Martínez-Sobrido, Texas Biomedical Institute, for the kind gift of mouse monoclonal SARS-CoV N antibody 1C7. Histopathology of human airway cultures was performed by Mark Alu, Branka Brukner Dabovic and Cynthia Loomis from the NYUMC Experimental Pathology Research Laboratory, which is supported by the Cancer Center Support Grant P30CA016087 at NYU Langone's Laura and Isaac Perlmutter Cancer Center. Statistical analysis of antiviral activities in $A549^{+ACE2}$ cells was performed by Woodrow Burchett. Research was further supported by grants from NIH/NIAID (R01AI143639 and R21AI139374 to MD, T32AI17647 to RAP), by Jan Vilcek/David Goldfarb Fellowship Endowment Funds to AMVJ, by Pfizer Inc. to MD, and by NYU Grossman School of Medicine Startup funds to MD.

Author contributions

MdV, ASM, JB, ASA, and MD conceived and designed the study. MdV, ASM, AMVJ, RAP performed the experiments and analyzed the data. CS, RO, JB analyzed antiviral data. MdV, ASM, AMVJ, RAP, LD, JB, MD interpreted the data. MdV, ASM, LD, and MD wrote the paper.

Competing interests

M. D. received a contract from Pfizer Inc. to support the studies reported herein. These authors are employees of Pfizer Inc. and hold stock in Pfizer Inc: Joseph Binder, Annaliesa Anderson, Claire Steppan, Rebecca O'Connor.

Materials and correspondence

All correspondence and material requests except those for antiviral compounds should be addressed to Meike.Dittmann@nyulangone.org. Compound requests should be addressed to Annaliesa.Anderson@pfizer.com.